Real-world evaluation of a self-startup SSHI rectifier for piezoelectric vibration energy harvesting

Sijun Du [a,*], Yu Jia [a,b], Chun Zhao [a], Shao-Tuan Chen [a], Ashwin A. Seshia [a]

[a] *Nanoscience Centre, Department of Engineering, University of Cambridge, Cambridge CB2 1PZ, UK*
[b] *Department of Mechanical Engineering, University of Chester, Chester CH2 4NU, UK*

ABSTRACT

This paper presents an enhanced SSHI (synchronized switch harvesting on inductor) rectifier with startup circuit and representative environment validation using real world vibration data collected from a tram. Compared to a conventional SSHI rectifier, the proposed rectifier dynamically monitors the working status of the circuit and restarts it when necessary. The proposed rectifier is designed in a $0.35\,\mu m$ HV CMOS process and its performance is experimentally evaluated. With a 500-s real-world collected vibration data, the conventional and the proposed SSHI rectifiers record average power performance improvements by $9.2\times$ and $22\times$ respectively, compared to a passive full-bridge rectifier. As the startup circuit helps restart the SSHI rectifier several times, it is able to extract energy in an increased excitation range and its average power output performance is $2.4\times$ higher than a conventional SSHI rectifier.

© 2017 The Authors. Published by Elsevier B.V. This is an open access article under the CC BY license (http://creativecommons.org/licenses/by/4.0/).

1. Introduction

As the Internet of Everything (IoE) continues to emerge, powering billions of distributed sensors becomes a big challenge. In the past decade, harvesting ambient vibration energy to power wireless sensor nodes and portable or wearable devices has attracted much research interest [1,2]. Harvested electrical power for most of MEMS or macroscopic harvesters varies from 10's μW to 10's mW depending on the scale and structure of harvesters [3,4]. Although the raw electrical output power is promising to power most low-power sensors, the stable DC electrical power, ready to be used for loads, significantly depends on the performance of the interface circuit to be employed [5,6].

Full-bridge rectifiers (FBR) are commonly used in commercial energy harvesting systems and the circuit diagram is shown in Fig. 1 [7–9]. The piezoelectric transducer (PT) is modeled as a current source I_P in parallel with a capacitor C_P and a resistor R_P. The FBR contains four diodes with a forward voltage drop noting as V_D and a storage capacitor C_S. In the associated waveforms, V_{PT} is the voltage across the PT. It can be seen that V_{PT} needs to flipped from $-(V_S+2V_D)$ to V_S+2V_D, or vice-versa, to overcome the threshold set by the FBR to transfer energy to C_S. Hence, the energy (or electrical charge) used to charge the internal capacitor C_P between these two voltages levels is wasted. The wasted charge is shown as black areas

in the waveform. If the excitation vibration level is low such that $V_{OC(pp)} < 2(V_S+2V_D)$, all harvested energy is wasted, where $V_{OC(pp)}$ is the open-circuit peak-to-peak voltage of V_{PT}. If $V_{OC(pp)}$ marginally overcomes the threshold, most of harvested energy is wasted and the power efficiency in this case is extremely low.

In order to increase the power extraction efficiency, many active rectifiers have been introduced to use inductors to improve the performance [10–15]. SSHI (synchronized switch harvesting on inductor) is one of the most efficient rectifiers using an RLC loop to synchronously flip the voltage V_{PT}, hence increase the power efficiency [16–19]. Fig. 2 shows the circuit diagram and associated waveforms of an SSHI rectifier. The inductor is controlled by analog switches, which are driven by a synchronous pulse signal ϕ_{SSHI}. From the waveform, it can be seen that a ϕ_{SSHI} pulse is generated for each zero-crossing moment of I_P. During the pulse of ϕ_{SSHI}, V_{PT} is flipped in the RLC system with some loss due to the parasitic resistance. As the RLC oscillation loop helps flip V_{PT}, the wasted charge, shown as black areas, is significantly decreased.

Fig. 3a shows a simplified architecture of an SSHI rectifier, which contains a FBR, a zero-crossing detection block, a pulse generation block and a level-shifter. When I_P is close to zero, the diodes of the FBR are just about to turn OFF. At this moment, one of V_P and V_N begins to increase from $-V_D$ and the other one begins to decrease from V_S+V_D. One common method to detect the zero-crossing moment of I_P is using two comparators to compare V_P and V_N with a reference voltage V_{ref}. This reference voltage is set slightly higher than $-V_D$ and it aims to finds the moment while V_P or V_N begins to increase from $-V_D$. The outputs of the two comparators

* Corresponding author.
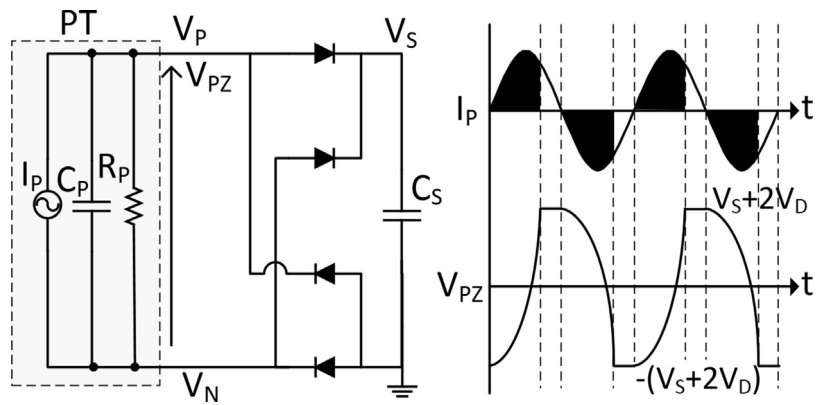 *E-mail addresses:* sd672@cam.ac.uk, sijundu@hotmail.com (S. Du).

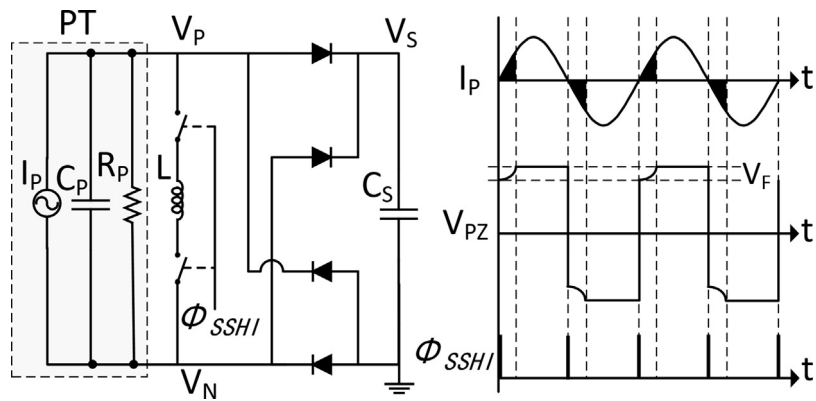**Fig. 1.** Full-bridge rectifier and the associated waveforms.

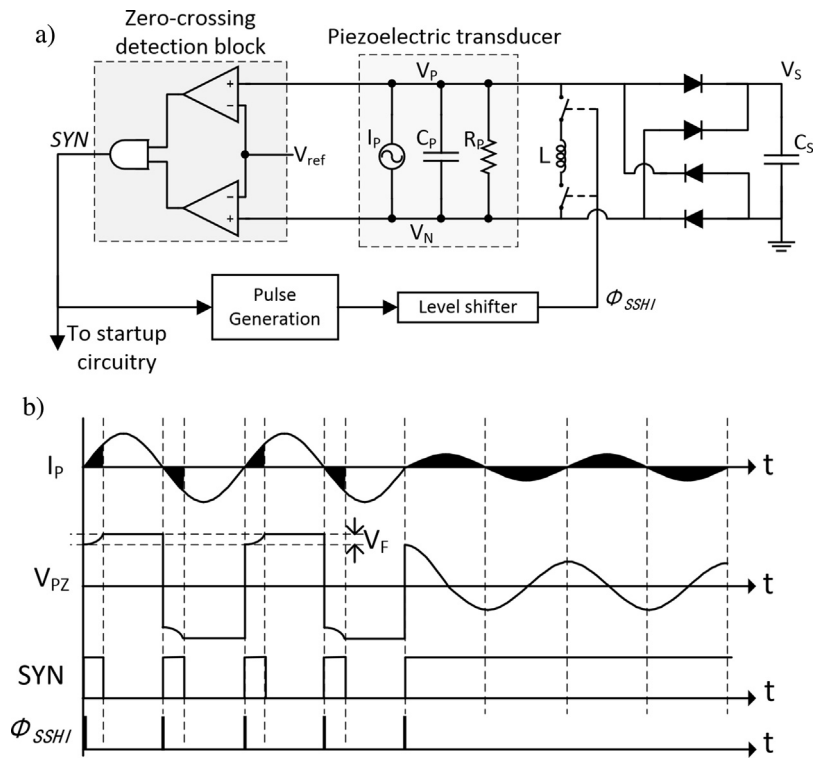**Fig. 2.** SSHI rectifier and the associated waveforms.

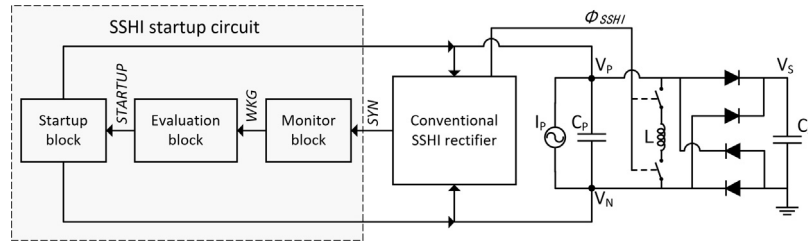**Fig. 3.** Circuit diagram of an SSHI rectifier and the associated waveforms.

Fig. 4. Architecture of the proposed SSHI rectifier with self-startup.
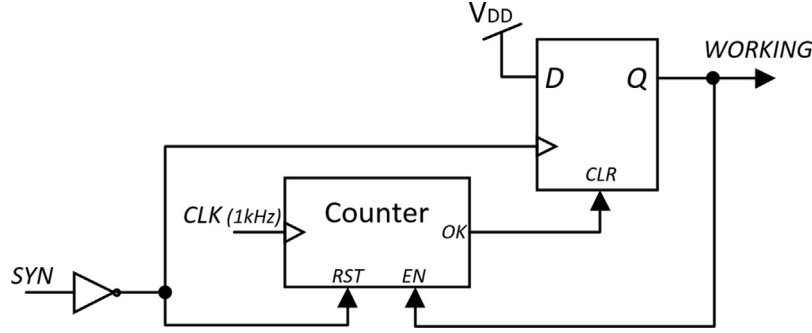

Fig. 5. Circuit diagram of the monitoring block.

are ANDed and the resulting signal *SYN* presents a synchronous signal to control the switch. For each zero-crossing moment of I_P, a rising edge is generated in *SYN* and it is used to generate a pulse in the following blocks to control the inductor. In the proposed rectifier, *SYN* is also used in a startup circuit, which will be presented in the next section.

The voltage loss after the flip is noted as V_F, as shown in Fig. 2, which depends on the inductance, parasitic resistance and C_P and it can be expressed as $V_F = (V_S + 2V_D)\left(1 - e^{-\frac{\pi}{\sqrt{\frac{4L}{R^2C}-1}}}\right)$. In order to keep generating rising edges in *SYN*, V_{PT} needs to attain $V_S + 2V_D$ or $-(V_S + 2V_D)$. Hence the condition for the SSHI rectifier to sustain operation is:

$$V_{OC(pp)} > V_F \qquad (1)$$

Fig. 3b shows the waveforms of the conventional SSHI rectifier. The SSHI rectifier is operating well while the excitation level satisfies the condition in (1). However, while the excitation goes to a near-zero level for a period of time, both V_P and V_N tends to $\frac{1}{2}V_S$ and they oscillate near this value if weak excitation is present. During this time, V_{PZ} tends to zero. In this case, *SYN* keeps high and there is no rising edge generated to flip V_{PT}. In order to start flipping V_{PT} again for each zero-crossing moment of I_P, either V_P or V_N should attain $-V_D$ to trigger one of the two comparators in the zero-crossing detection block. This is also the condition that V_{PT} attains $V_S + 2V_D$ or $-(V_S + 2V_D)$. Hence, after the SSHI rectifier stops working, the condition for it to restart is:

$$V_{OC(pp)} > 2(V_S + 2V_D) \qquad (2)$$

Comparing the two conditions in (1) and (2), the condition to restart is much more difficult to be satisfied than the condition to sustain. Hence, the vibration energy between these two excitation levels is completely wasted for conventional SSHI rectifiers if it is not started [20]. This paper proposed an enhanced SSHI rectifier with a startup circuit and the fabricated chip is experimentally evaluated with a 500-s real-world collected vibration data from a tram in Birmingham, UK. The real-world performance of the con-

ventional SSHI and proposed SSHI circuits are compared to see the obvious improvement by adding a startup circuit.

2. Proposed SSHI rectifier

Fig. 4 shows the block architecture of the proposed SSHI rectifier with startup circuit, which consists of a conventional SSHI rectifier and a startup circuit. The startup circuit contains three main blocks: monitoring block, evaluation block and startup block. The monitoring block monitors the working status of the conventional SSHI rectifier and it outputs a signal *WKG* indicating if the voltage across the piezoelectric transducer (PT), V_{PT}, is being correctly flipped for each zero-crossing moment. If *WKG* goes low, the evaluation block starts evaluating the ambient excitation level and stability to determine when the SSHI rectifier needs to be restarted. Once it confirms that a startup operation can be performed, a *STARTUP* signal is generated to let the following startup block to restart the SSHI rectifier.

The circuit diagram of the monitoring block is shown in Fig. 5, where there are a digital counter and a D-flip-flop. While the SSHI rectifier is working, *SYN* goes high and low periodically and it resets the counter and sets the output *WKG* to high. While the SSHI rectifier is not working, *SYN* stays high. In this case, the counter cannot be reset until it counts to a preset value, which reset *WKG* to low level indicating that the SSHI rectifier is not working.

Fig. 6 shows the circuit implementation of the evaluation block, which evaluates the excitation level and excitation stability. (1) indicates the condition for a conventional SSHI rectifier to keep working. Hence, this condition should first be satisfied before restarting the SSHI. This evaluation is performed in the stage 1 by comparing fractions of V_P and V_S. The condition in (1) can be rewritten as $V_P > \frac{1}{2}V_S + \frac{1}{4}V_F$ or $V_P < \frac{1}{2}V_S - \frac{1}{4}V_F$ because $V_{PT} = V_P - V_N$ and both V_P and V_N are centered at $\frac{1}{2}V_S$. Choosing $V_P < \frac{1}{2}V_S - \frac{1}{4}V_F$ as the evaluation condition, it can be further rewritten as:

$$V_P < \frac{1}{2}V_S - \frac{V_S}{4}\left(1 - e^{-\frac{\pi R}{2}\sqrt{\frac{C}{L}}}\right) \Rightarrow V_P < \frac{1}{4}V_S\left(1 + e^{-\frac{\pi R}{2}\sqrt{\frac{C}{L}}}\right) \qquad (3)$$

The forward voltage V_D is assumed to be negligible compared to V_S. Assuming $C_P = 45$ nF, the total ON resistance of the RLC loop is $R = 20\,\Omega$ and the inductor is 1 mH, (3) can be approximated as $\frac{1}{2}V_P <$
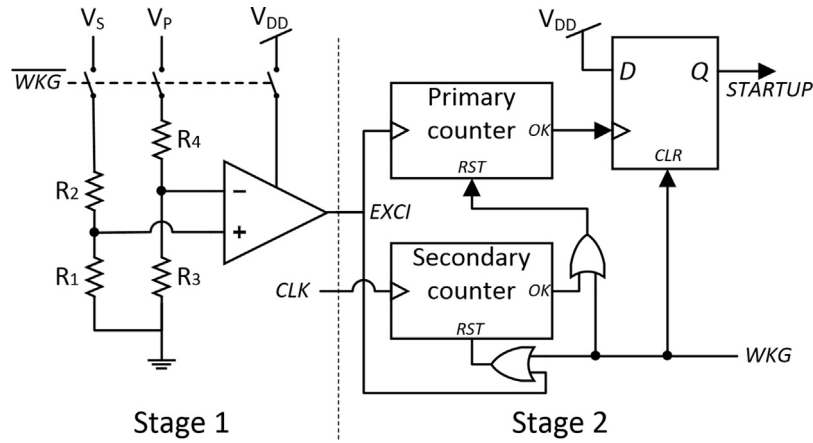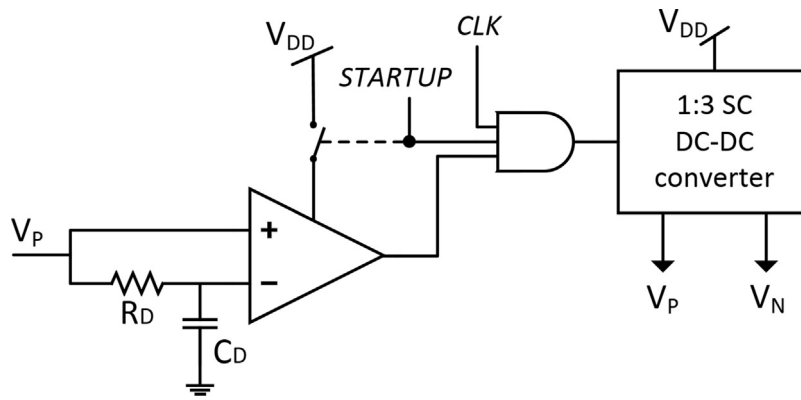
Fig. 6. Circuit diagram of the evaluation block.

Fig. 7. Circuit diagram of the startup block.

$\frac{3}{16}V_S$. Hence, the resistors shown in Fig. 6 are chosen as $R_1 = 60\,\mathrm{M\Omega}$, $R_2 = 260\,\mathrm{M\Omega}$, $R_3 = R_4 = 50\,\mathrm{M\Omega}$ and they are off-chip implemented.

The second stage aims to evaluate if the excitation is stable because an impulse excitation will not keep the SSHI rectifier working for a long time and, in this case, it does not worth to waste energy to restart the SSHI circuit. In this stage, two digital counters are employed. The primary counter counts the number of periods of the high excitation and the secondary counter is used to reset the primary counter to make it ready for the next counting. If the excitation is high and stable, the signal $EXCI$ will continue drive the primary counter until it counts to a preset value. Then the following D-flip-flop outputs a high $STARTUP$ to the next block. If the excitation is not stable, $EXCI$ signal will stop before the primary counter finishes and, after a period of time counted in the secondary counter, the primary counter will be reset.

Fig. 7 shows the startup block. This block is controlled by the signal $STARTUP$ from the previous block. Once $STARTUP$ goes high, the comparator is powered. While V_P attains its minimum value and tries to increase, the output of the comparator goes high and enable the clock signal CLK. The signal CLK drives a 1:3 switched capacitor DC-DC converter to charge the voltage $V_P - V_N$, which is also V_{PT}, to a much higher value until $V_{PT} = V_S + 2V_D$. This operation is similar to flipping V_{PT} but with a large absolute gain. While V_{PT} attains $V_S + 2V_D$, the voltage V_N equals $-V_D$ and one comparator in the zero-crossing detection block (Fig. 3a) is triggered to generate a SYN signal. The SYN signal is then acknowledged by the monitoring block and a high level of WKG signal is generated to disable all other blocks in the startup circuit. As the signal SYN is generated, the voltage across the PT can now be correctly flipped and the SSHI rectifier restarts working.

In some cases the SSHI rectifier can be self-started without using the proposed startup circuit. If the shock or excitation level is high such that the condition in (2) is met, a SYN signal will instantly be generated and the WKG signal goes to high immediately. In this case, the conventional SSHI circuit is self-started without using the startup circuit. However, as previously mentioned, the excitation level required to satisfy (2) is very high, so self-startup is very hard to be achieved in real-world implementations. Experiments with a real-world vibration source will present how the proposed startup circuit improve the overall energy efficiency in the next section.

3. Measurement results

The proposed rectifier is designed and fabricated in 0.35 μm HV CMOS process and the die photo is shown in Fig. 8. The proposed rectifier contains a conventional SSHI rectifier and a startup circuit. Hence experiments on both the conventional and the proposed SSHI can be performed with the chip by disabling and enabling the startup circuit to compare the performance. The power consumption of the chip is 0.8 μW while the SSHI rectifier is operating. After the SSHI rectifier stops operation, the consumption goes down to 0.65 μW as the voltage-flipping signal ϕ_{SSHI} is not generating in this case to drive the analog switches.

Unlike majority of the previous work in the literature, experimental measurements did not simply employ a sine wave excitation in order to realize the representative environment validation. This is because real-world ambient vibration is rarely that of a pure sine wave, and is typically broadband, noisy and time-varying in nature. Hence, performing experiments with real-world collected data can better present the performance improvement
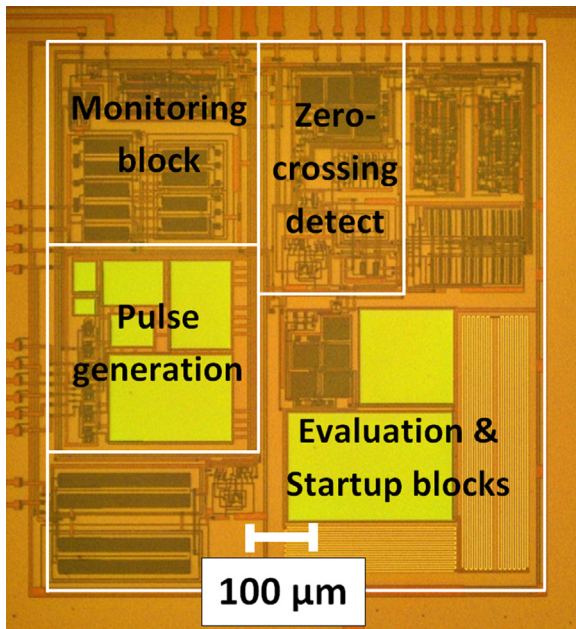
Fig. 8. Die photo of the proposed SSHI rectifier.

of the proposed SSHI rectifier compared to the full-bridge rectifier and the conventional SSHI rectifiers.

Fig. 9 shows the vibration data collected from the undercarriage of a tram in Birmingham, United Kingdom. The data was measured using a digital accelerometer (Analog Devices ADXL345) integrated with a data logger (Gulf Coast X16-2) with a sampling rate at 400 Hz. The data lasts for 500 s and it can be seen that it is very noisy and the vibration amplitude randomly varies with time. Eight time moments, t_1 to t_8, are labeled in the figure to facilitate explanations. The two zoomed-in figures shows short periods at 35 s and 75 s while the tram is stationary and moving, respectively. Fig. 10 shows the STFT (Short-time Fourier Transform) plot of the vibration data. Comparing the two figure, it can be seen that the low amplitude periods (t_1, t_3, t_6 and t_8) shown in Fig. 9 represents the time while the tram stops. These are either due to tram stations (t_1, t_3 and t_8) or traffic lights (t_6). It can be observed from the STFT plot that while the tram is moving, the vibration frequency is centered and peaked at around 65 Hz; however, while the tram stops, the vibration is very noisy and is no longer centered to any specific frequencies. This phenomena can also be observed from the two zoomed-in figures in Fig. 9. While the tram is stationary (left sub-figure), the captured acceleration data is very noisy and while the tram is moving (right sub-figure), the data looks more like a sinusoidal signal of frequency around 65 Hz with a little noise. In terms of the vibration amplitude, it varies for different periods while the tram is moving. For example, the amplitudes at t_2, t_6 and t_7 are relatively low but the amplitude at t_4 is much higher. This can be due to rail track conditions and the speed of the tram.

The measurements were performed using a commercially available cantilevered piezoelectric harvester (Mide Technology V20W) with the nature frequency of 82 Hz. In order to use this piezoelectric transducer (PT) with the vibration data shown in Fig. 10, the natural frequency of this PT was tuned to 65 Hz by adding a tiny tip mass. Fig. 11 shows the experimental setup. The 500-s vibration data was downloaded into a waveform generator (Agilent Technologies 33250A 80 MHz waveform generator) and the signal was amplified by a power amplifier (LDS PA100E Power Amplifier) to match the acceleration level with the real-world vibration. The modified piezoelectric harvester was then excited on a shaker (LDS V406 M4-CE) driven by the signal to test different interface circuits.

First, the vibration data is used to measure the performance of a passive full-bridge rectifier (FBR). As the threshold to extract energy for a FBR is high as given in (2), only the short period with high excitation level (around t_4 in Fig. 9) attains the threshold. However, as most of energy is wasted due to flipping the voltage, the power efficiency is extremely low in this case. Measurements show that V_S is increased from 2.91 V to 2.96 V in this 500-s measurement. C_S is a super capacitor (AVX BestCap BZ05CA103ZSB) with measured capacitance $C_S = 5.2$ mF, so the energy extracted in this 500 s is $\frac{1}{2}C_S(2.96^2 - 2.91^2) = 0.76$ mJ and the average power over the 500 s is 1.53 μW.

In order to make fair comparisons of different circuits, V_S is set to be around 3 V before charging starts. Although different circuits require different V_S values to achieve their maximum power points (MPP) and $V_S \approx 3$ V may not be the optimal value, the initial value $V_S \approx 3$ V is chosen because it is believed to be around the preferred supply voltages of most wireless sensors, which require stable DC supplies between 1.8 V and 5 V.

The conventional SSHI rectifier without startup circuit is then tested. Fig. 12 shows measured waveforms for 500 s. The signal V_P is the voltage at one electrode of the harvester. ϕ_{SSHI} is the inductor-control signal to flip the voltage across the harvester. WKG is the signal indicating if the SSHI rectifier is working and V_S is the voltage across the storage capacitor C_S connected at the output of the full-bridge rectifier. These signals are also labeled in Fig. 4.

At t_1, the SSHI rectifier is not working as the tram stops; hence, ϕ_{SSHI} is not generated, WKG keeps at low and no energy is transferred into C_S. Although the tram starts moving at t_2, the condition for the conventional SSHI to start working is still not satisfied as the required excitation level is high as shown in (2). At t_4, the tram starts moving again and the excitation level at this moment is high (refer to t_4 in Fig. 9). The condition in (2) is satisfied and the conventional SSHI rectifier is started. Therefore, the voltage across the PT is correctly flipped by the signal ϕ_{SSHI} and WKG goes high. V_S is also increased as charge flows into C_S. From Fig. 9, it can be seen that, after a short period of high excitation, the excitation level is decreased at t_5 although the tram still keeps moving. However, the conventional SSHI rectifier does not stop working because it is already started and the condition to sustain its operation is much lower as expressed in (1). Then the tram stops due to the traffic lights at t_6 and the rectifier stops working. Once the SSHI rectifier stops working, the condition to restart it is now again difficult to be satisfied. Hence, the following moderate excitation level after the tram starts moving at t_7 cannot restart the conventional SSHI rectifier and the vibration energy during this period is wasted.

During this 500 s measurement, the storage capacitor C_S is charged from 2.99 V to 3.43 V. Hence, the energy extracted by the circuit is $\frac{1}{2}C_S(3.43^2 - 2.99^2) = 7.344$ mJ and the average electrical power over the 500 s is 14.68 μW. In addition, as previously measured, the power consumption of the chip is 0.8 μW while SSHI is operating and 0.65 μW while SSHI is not operating. The average power consumption in this 500 s can be estimated to be around 0.68 μW by estimating the duty ratio while SSHI is operating (high WKG signal). Hence, the net output power by a conventional SSHI rectifier is around 14 μW.

The same vibration data is used again to test the proposed SSHI rectifier with startup circuit. Fig. 13 shows the waveforms, where there are five signals. The signals are labeled in the system architecture in Fig. 4 and the last signal $STARTUP$ is the signal sent to the startup block to restart the SSHI circuit. From the signal V_P, it can be seen that there is a short impulse at the beginning. As this impulse is too short, the evaluation block (Fig. 6) does not approve a restart operation. The tram starts moving from t_1 and the evaluation block begins to evaluate the amplitude and duration of the excitation. After a short period of time at t_2, the excitation is evaluated as high and stable; hence a $STARTUP$ pulse is generated and
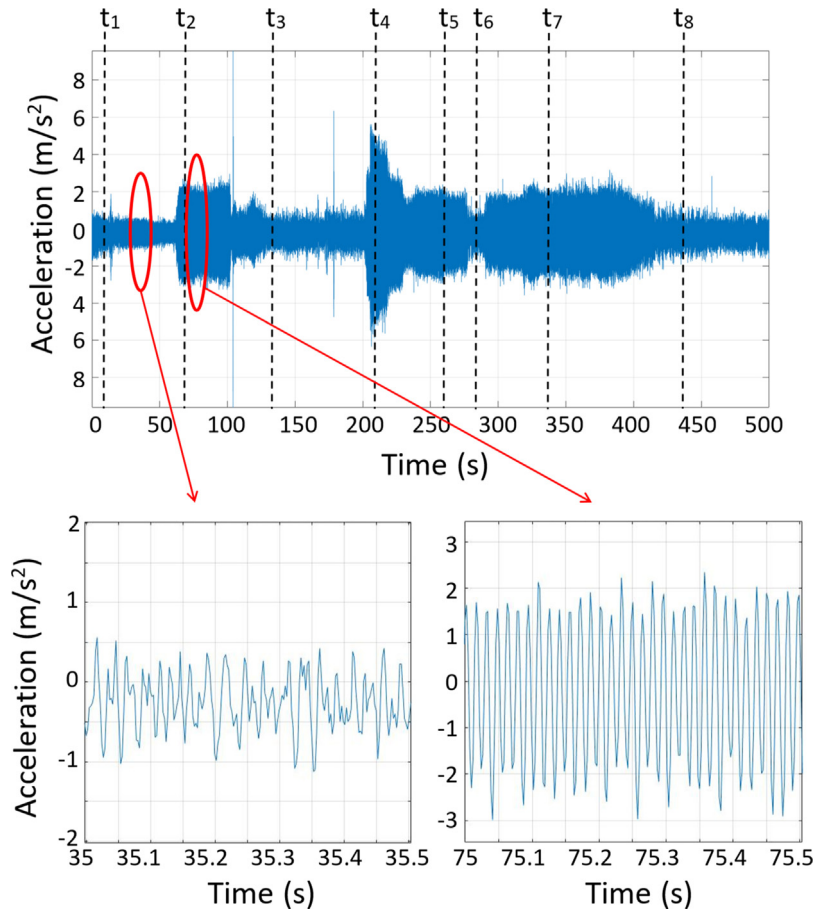
Fig. 9. Time-domain acceleration plots of the measured real-world vibration data of length 500 s collected from a tram in Birmingham, UK.
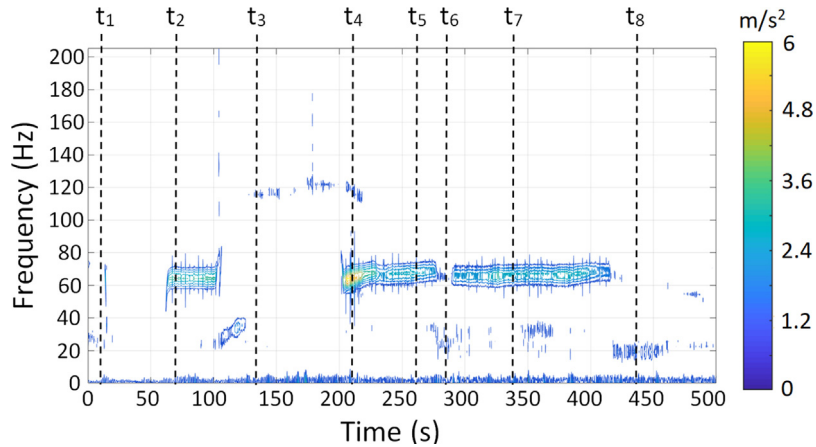

Fig. 10. STFT (Short-time Fourier Transform) plot of the vibration data.

the SSHI rectifier is restarted. During the remaining time while the tram is moving, *WKG* keeps high and ϕ_{SSHI} pulses are generated to flip the voltage until the tram stops. At t_3, the tram starts moving again. As the excitation level at this moment is sufficiently high so that the condition in (2) is satisfied, the SSHI rectifier is directly self-started without using the startup circuit. The startup mechanism at this moment is the same as the conventional SSHI rectifier. Hence, neither the short evaluation period nor the *STARTUP* pulse is present at this time. During the short stop of waiting for traffic lights, the SSHI rectifier stops working again. While the tram starts moving at t_4, the startup circuit starts evaluating the excitation and another *STARTUP* pulse is generated at t_5 to restart the SSHI rectifier.

During the 500 s measurement, V_S is increased from 2.92 V to 3.89 V, hence the extracted energy is calculated as 17.2 mJ and the average power is 34.4 μW. In addition, the average quiescent power consumption of the chip in this 500 s is estimated to be around 0.73 μW. Therefore, the net output power of the proposed SSHI rectifier is 33.67 μW.

4. Conclusion

This paper proposes an enhanced SSHI rectifier with startup circuits and it is implemented in a real-world vibration environment. The chip is designed in a 0.35 μm CMOS process. Instead of using
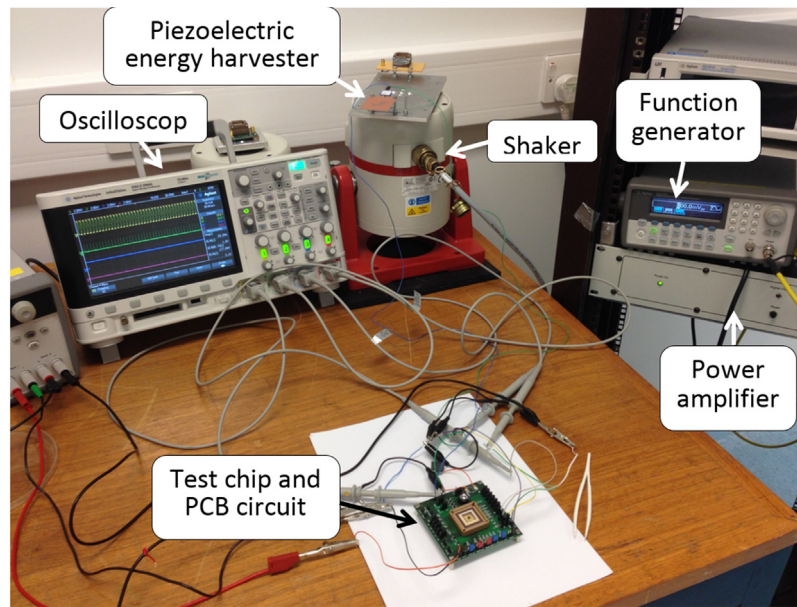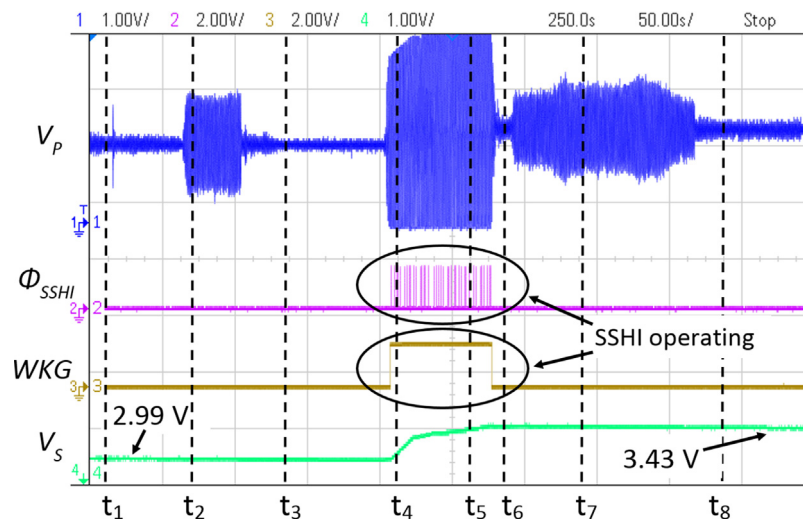
Fig. 11. Experimental setup.

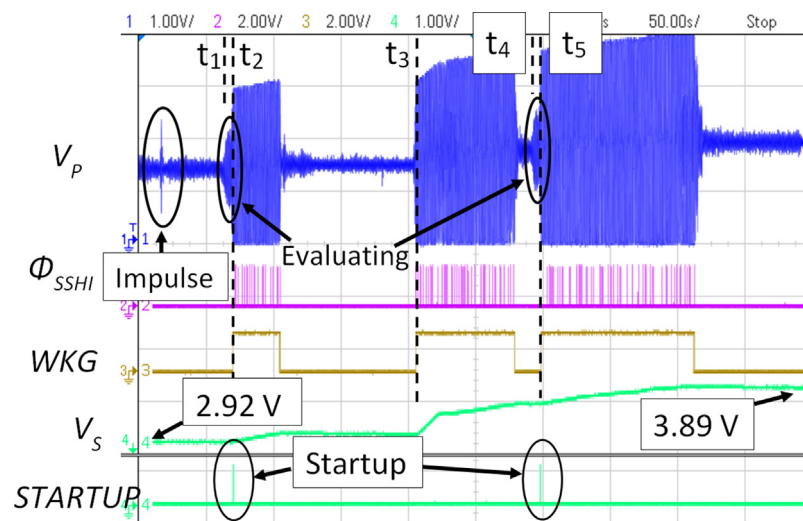**Fig. 12.** Waveforms of the conventional SSHI rectifier.

Fig. 13. Waveforms of the proposed SSHI rectifier with startup circuit.

a sine wave excitation signal, the chip is experimentally evaluated under the excitation of a 500-s real-world collected vibration data from a tram in Birmingham, UK. The real-world vibration data is much noisier than a sine wave signal and the excitation level is highly unpredictable. The measured results shows that the proposed SSHI rectifier is able to operate in an increased excitation range and extract more power compared to conventional SSHI rectifiers. During the 500 s measurements, the startup circuit helps the SSHI rectifier restart twice and the total extracted energy is $2.4\times$ higher than the conventional SSHI circuit. Compared to a passive full-bridge rectifier, the conventional and the proposed SSHI rectifiers improve the performance by $9.2\times$ and $22\times$, respectively.

Funding

References

[1] P.D. Mitcheson, E.M. Yeatman, G.K. Rao, A.S. Holmes, T.C. Green, Energy harvesting from human and machine motion for wireless electronic devices, Proc. IEEE 96 (9) (2008) 1457–1486.

[2] A. Harb, Energy harvesting: state-of-the-art, Renew. Energy 36 (10) (2011) 2641–2654.

[3] S.P. Beeby, M.J. Tudor, N.M. White, Energy harvesting vibration sources for microsystems applications, Meas. Sci. Technol. 17 (12) (2006) R175.

[4] J. Lee, B. Choi, Development of a piezoelectric energy harvesting system for implementing wireless sensors on the tires, Energy Convers. Manage. 78 (2014) 32–38.

[5] T.T. Le, H. Jifeng, A. von Jouanne, K. Mayaram, T.S. Fiez, Piezoelectric micro-power generation interface circuits, IEEE J. Solid-State Circuits 41 (6) (2006) 1411–1420.

[6] A. Khaligh, Z. Peng, Z. Cong, Kinetic energy harvesting using piezoelectric and electromagnetic technologies 2014;state of the art, IEEE Trans. Ind. Electron. 57 (3) (2010) 850–860.

[7] G.D. Szarka, B.H. Stark, S.G. Burrow, Review of power conditioning for kinetic energy harvesting systems, IEEE Trans. Power Electron. 27 (2) (2012) 803–815.

[8] J. Qiu, H. Jiang, H. Ji, K. Zhu, Comparison between four piezoelectric energy harvesting circuits, Front. Mech. Eng. China 4 (2) (2009) 153–159.

[9] L.M. Miller, A.D.T. Elliott, P.D. Mitcheson, E. Halvorsen, I. Paprotny, P.K. Wright, Maximum performance of piezoelectric energy harvesters when coupled to interface circuits, IEEE Sens. J. 16 (12) (2016) 4803–4815.

[10] M. Dini, A. Romani, M. Filippi, M. Tartagni, A nanopower synchronous charge extractor ic for low-voltage piezoelectric energy harvesting with residual charge inversion, IEEE Trans. Power Electron. 31 (2) (2016) 1263–1274.

[11] S. Du, Y. Jia, A.A. Seshia, An efficient inductorless dynamically configured interface circuit for piezoelectric vibration energy harvesting, IEEE Trans. Power Electron. 32 (5) (2017) 3595–3609.

[12] E.E. Aktakka, K. Najafi, A micro inertial energy harvesting platform with self-supplied power management circuit for autonomous wireless sensor nodes, IEEE J. Solid-State Circuits 49 (9) (2014) 2017–2029.

[13] D. Kwon, G.A. Rincon-Mora, A single-inductor 0.35 μm CMOS energy-investing piezoelectric harvester, IEEE J. Solid-State Circuits 49 (10) (2014) 2277–2291.

[14] N. Kong, D.S. Ha, Low-power design of a self-powered piezoelectric energy harvesting system with maximum power point tracking, IEEE Trans. Power Electron. 27 (5) (2012) 2298–2308.

[15] T. Hehn, F. Hagedorn, D. Maurath, D. Marinkovic, I. Kuehne, A. Frey, Y. Manoli, A fully autonomous integrated interface circuit for piezoelectric harvesters, IEEE J. Solid-State Circuits 47 (9) (2012) 2185–2198.

[16] A. Badel, D. Guyomar, E. Lefeuvre, C. Richard, Efficiency enhancement of a piezoelectric energy harvesting device in pulsed operation by synchronous charge inversion, J. Intell. Mater. Syst. Struct. 16 (10) (2005) 889–901.

[17] L. Shaohua, F. Boussaid, A highly efficient P-SSHI rectifier for piezoelectric energy harvesting, IEEE Trans. Power Electron. 30 (10) (2015) 5364–5369.

[18] Y.K. Ramadass, A.P. Chandrakasan, An efficient piezoelectric energy harvesting interface circuit using a bias-flip rectifier and shared inductor, IEEE J. Solid-State Circuits 45 (1) (2010) 189–204.

[19] J. Liang, W.-H. Liao, Improved design and analysis of self-powered synchronized switch interface circuit for piezoelectric energy harvesting systems, IEEE Trans. Ind. Electron. 59 (4) (2012) 1950–1960.

[20] S. Du, Y. Jia, C.D. Do, A.A. Seshia, An efficient SSHI interface with increased input range for piezoelectric energy harvesting under variable conditions, IEEE J. Solid-State Circuits 51 (11) (2016) 2729–2742.

Biographies

Sijun Du received the B.Eng. degree in electrical engineering from University Pierre and Marie Curie, Paris, France, in 2011 and the M.Sc. degree in Electrical Electronics Engineering from Imperial College, London, U.K., in 2012. He worked at the Laboratory LIP6 of University Pierre Marie Curie, Paris, and then worked as a digital IC engineer in Shanghai between 2012 and 2014. He is currently working towards the Ph.D. Degree at the University of Cambridge, U.K., where he is affiliated with the Cambridge Nanoscience Centre. His research interests include energy harvesters and associated interfaces, power electronics, power management circuits, DC-DC converters and rectification circuits.

Yu Jia is currently a Lecturer in Mechanical Engineering at the University of Chester, and leads the Smart Microsystems Research Group. Yu Jia received a First Class (Honours) degree in MEng Electromechanical Engineering from the University of Southampton in 2010, and PhD in Engineering from the University of Cambridge in 2014. He was then a Research Associate at Cambridge for a year. He is the co-founder of 8power Ltd. He is also a steering board member of the Energy Harvesting Network. His research interests involve vibration energy harvesting, micro-electromechanical systems, nonlinear vibration dynamics and smart integrated systems.
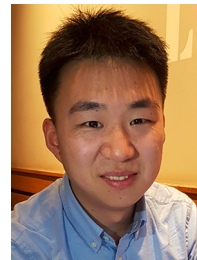
Chun Zhao received the B.Eng. degree in measurement and control technology and instrument from the Huazhong University of Science and Technology, Wuhan, China, in 2009; the M.Sc. degree in analog and digital IC design from Imperial College London, London, U.K., in 2011; and the Ph.D. degree in microelectromechanical systems (MEMS) from the University of Southampton, Southampton, U.K., in 2016. From April 2015 to March 2016, he was a full time Research Scientist at Sharp Laboratories of Europe, Oxford, U.K., working on the research and development of acoustic MEMS devices and integrated control circuit design. He joined the Department of Engineering, University of Cambridge in April 2016, where he is currently a Research Associate in MEMS. His current research interests include MEMS, microresonators, miniature sensors (such as inertial sensors) and actuators, MEMS energy harvesting, MEMS system modelling and interface circuit for sensors design.

Shao-Tuan Chen received the B.S. degree in Mechanical engineering from National Taiwan University, Taiwan, in 2013 and the MPhil. Degree in Electrical Engineering from University of Cambridge, U.K., in 2015. He is currently working towards the Ph.D. Degree at the University of Cambridge, U.K., where he is affiliated with the Cambridge Nanoscience Centre. His research interests include nonlinear vibration energy harvesting and the reliability and robustness designs for MEMS (Microelectromechanical Systems) energy harvesters, and the associated nonlinear system identification for MEMS vibration energy harvesters.

Ashwin A. Seshia received his BTech in Engineering Physics in 1996 from IIT Bombay, MS and PhD degrees in Electrical Engineering and Computer Sciences from the University of California, Berkeley in 1999 and 2002 respectively, and the MA degree in engineering from the University of Cambridge in 2008. During his time at the University of California, Berkeley, he was affiliated with the Berkeley Sensor & Actuator Center. He joined the faculty of the Engineering Department at the University of Cambridge in October 2002 where he is presently a Reader in Microsystems Technology and a Fellow of Queens' College. He is a Fellow of the Institute of Physics, a Fellow of the Institution for Engineering and Technology and a senior member of the Institute of Electrical and Electronics Engineers. His research interests are in the domain of microengineered dynamical systems with applications to sensors and sensor systems. He serves on the editorial boards of the IEEE Journal of Microelectromechanical systems, the IOP Journal of Micromechanics and Microengineering, the IEEE Transactions on Nanotechnology and the IEEE Transactions on Ultrasonics, Ferroelectrics and Frequency Control.